

# Journal of Materials Chemistry A

Accepted Manuscript



This is an *Accepted Manuscript*, which has been through the Royal Society of Chemistry peer review process and has been accepted for publication.

*Accepted Manuscripts* are published online shortly after acceptance, before technical editing, formatting and proof reading. Using this free service, authors can make their results available to the community, in citable form, before we publish the edited article. We will replace this *Accepted Manuscript* with the edited and formatted *Advance Article* as soon as it is available.

You can find more information about *Accepted Manuscripts* in the [Information for Authors](#).

Please note that technical editing may introduce minor changes to the text and/or graphics, which may alter content. The journal's standard [Terms & Conditions](#) and the [Ethical guidelines](#) still apply. In no event shall the Royal Society of Chemistry be held responsible for any errors or omissions in this *Accepted Manuscript* or any consequences arising from the use of any information it contains.

## High performance microspherical activated carbons for methane storage and landfill gas or biogas upgrade†

Ana S. Mestre<sup>a,b\*</sup>, Cristina Freire<sup>b</sup>, João Pires<sup>a</sup>, Ana P. Carvalho<sup>a</sup>, Moisés L. Pinto<sup>c\*</sup>

<sup>1</sup> *Centro de Química e Bioquímica, Faculdade de Ciências, Universidade de Lisboa, 1749-016 Lisboa, Portugal*

<sup>2</sup> *REQUIMTE, Departamento de Química e Bioquímica, Faculdade de Ciências, Universidade do Porto, 4169-007, Portugal*

<sup>3</sup> *Department of Chemistry, CICECO, University of Aveiro, 3810-193 Aveiro, Portugal*

\*Corresponding Author: Fax: +351 217500088. E-mail address: [asmestre@fc.ul.pt](mailto:asmestre@fc.ul.pt) (Ana S. Mestre) and [moises.pinto@ua.pt](mailto:moises.pinto@ua.pt) (Moisés L. Pinto)

† Electronic supplementary information (ESI) available: Details on analysis of  $\alpha_S$  plots and adsorption modelling; additional methane and carbon dioxide adsorption isotherms in the low pressure region at 25 °C. See DOI: xxx

**ABSTRACT**

Microspherical activated carbons were successfully prepared *via* a novel synthetic route that involves the hydrothermal carbonization of a renewable material, sucrose, and activation with  $K_2CO_3$ . The use of  $K_2CO_3$  resulted in better yields ( $\sim 50\%$ ) and the retention of the spherical shape of the hydrochar, while, with the less environmentally desirable and commonly used activating agent, KOH, the process occurs at the expense of the spherical morphology. The superior performance of the  $K_2CO_3$  activated samples for methane storage and upgrade of landfill gas or biogas results from the combination of several key properties including high packing densities ( $\sim 0.9\text{ g cm}^{-3}$ ), high surface areas (up to  $1400\text{ m}^2\text{ g}^{-1}$ ) and micropore sizes suitable for methane storage and selective  $CO_2/CH_4$  separation. In fact, the micropore size distributions assessed from  $CO_2$  adsorption data through a methodology not imposing a Gaussian distribution gave meaningful values to explain both the selectivity and storage capacity of samples. Sample activated with  $K_2CO_3$  at  $800\text{ }^\circ\text{C}$  with micropore sizes  $\sim 0.8\text{ nm}$ , and high packing density have high volumetric methane uptake ( $90\text{ (V/V)}$  at  $1000\text{ kPa}$ ), close to the best activated carbons reported in literature. Sample activated with  $K_2CO_3$  at  $700\text{ }^\circ\text{C}$  has narrower micropores ( $\sim 0.5\text{ nm}$ ) and presents remarkable selectivity ( $4 - 7$ ) in  $CO_2/CH_4$  mixtures for the upgrade of methane based fuels, like natural gas, landfill gas, and biogas. Although a superactivated carbon ( $\sim 2400\text{ m}^2\text{ g}^{-1}$ ) was obtained with KOH activation, the low packing density and wider micropores rendered it less effective for both methane storage and upgrade.

## Introduction

The searching of renewable energy sources is becoming increasingly important due to global warming and climate change effects are currently being more severe. In this context, fuels based on renewable sources, like landfill gas and biogas, which are rich in methane, need to be further explored regarding both production and use. Two main technological steps are involved in the spreading of these methane based fuels. The first is the purification or upgrading of the methane content on these gases and the second is methane storage at high densities and low to moderate pressures for easy application in the automotive industry. In the present work, we explore the merits of microspherical activated carbons prepared from a sucrose-based hydrochar for application in these two challenges.

Methane separation from carbon dioxide is the main step in the upgrading of natural gas, landfill gas and biogas to achieve fuel grade quality, and to avoid corrosion during transport and storage.<sup>1</sup> It is often mandatory to purify these gases before their use in high value applications because they may contain large amounts of carbon dioxide (40–65%).<sup>2–4</sup> Other contaminants are also present, although in lower concentrations, and are easier to separate from methane. For example, minimum fuel quality for compressed natural gas driven vehicles now corresponds to the G25 reference test fuel (85% methane, 14% nitrogen).<sup>5</sup> Thus, enrichment in methane is a pre-requisite, which is essentially achieved by carbon dioxide removal. Regarding landfill gas and biogas, prevention of their uncontrolled emission to the atmosphere is environmentally important because the global warming potential (GWP) of CH<sub>4</sub> is 21 times larger than that of CO<sub>2</sub>.<sup>6,7</sup> Separation studies of CH<sub>4</sub> from CO<sub>2</sub> by adsorption processes using several types of adsorbent materials, like alumina, activated carbons, zeolites and porous clays, was revised in the introduction of recent papers.<sup>8–10</sup>

Storage of methane by compression requires multi-stage compression up to 20 MPa to achieve a practical storage capacity in a given tank, implying expensive compression units and storage tanks, and considerable energy consumption. Another method of storage is gas adsorption at relatively low pressure in a lightweight cylinder filled with adsorbent material. This method is attractive because the adsorbent can be filled with the gas using and inexpensive single-stage compressor, thus demanding less energy consumption. Methane storage in activated carbons at low to moderate pressures has been considered as a very promising alternative to compression and their fundamental aspects are reasonably studied.<sup>11, 12</sup> Carbon materials have been successfully used in methane storage and landfill gas or biogas upgrading mainly due to their large specific surface areas, microporosity tailoring, and high packing densities. These properties are allied to the possibility of being produced from largely available renewable biomass, which make them less expensive than other microporous adsorbent materials (i.e. zeolites or metal organic frameworks).

Superactivated carbons, prepared by chemical activation with KOH of hydrochars obtained from hydrothermal carbonization (HTC) of carbohydrates, polysaccharides or biomass have shown very high adsorption capacities for CO<sub>2</sub> capture<sup>13, 14</sup> or CH<sub>4</sub> storage.<sup>13</sup> However, these materials have lower packing density than, for instance, anthracite-derived carbons with similar micropore networks,<sup>15</sup> being a disadvantage for their use in storage or separation processes, since an adsorbent with low packing density will request the use of bigger storage containers or separation towers.

Due to our experience in the use of K<sub>2</sub>CO<sub>3</sub> as activating agent,<sup>16-23</sup> recently we have been interested in extend our studies to the activation of spherical hydrochars with this compound aiming the preparation of spherical activated carbons.<sup>24</sup> K<sub>2</sub>CO<sub>3</sub> is an alternative to KOH with the advantage that carbonate mediated activation is less extensive

and is an environmental friendly activating agent<sup>25</sup> compared to  $\text{ZnCl}_2$ ,  $\text{H}_3\text{PO}_4$ , and  $\text{KOH}$ , the most commonly reported chemical activating agents.<sup>26</sup> So, to combine the development of the microporosity and the preservation of the hydrochar spherical morphology,  $\text{K}_2\text{CO}_3$  is a promising activating agent.

The objective of the present work was to test three sucrose-derived activated carbons for methane storage or upgrade from landfill gas or biogas. The samples were selected from a larger set of activated carbons prepared from hydrochars in order to have materials presenting high developed and tailored microporosity, preferentially allied with spherical morphology to attain high packing densities. The use of  $\text{K}_2\text{CO}_3$  as activating agent of spherical hydrochars proved to be crucial to obtain high performance adsorbents for methane storage and also for natural, landfill gas or biogas upgrade.

## Experimental

### Activated carbons preparation

The hydrochar was prepared introducing  $15 \text{ cm}^3$  of  $1.5 \text{ mol dm}^{-3}$  sucrose (Analar Normapur, > 99 %) aqueous solution in a Teflon-lined stainless steel autoclave. The autoclave was placed in an oven (Medline Scientific Limited, model ON-02G), which had been pre-heated at  $190 \text{ }^\circ\text{C}$  and hydrothermal carbonization (HTC) was performed during 5 h. The autoclave was cooled down to room temperature and the powder (hydrochar S) was washed with distilled water and acetone, and dried at  $60 \text{ }^\circ\text{C}$ . Activated carbon samples SC800 and SH800 were prepared with, respectively,  $\text{K}_2\text{CO}_3$  and  $\text{KOH}$ . The activation was performed by impregnating in solution ( $\sim 10 \text{ cm}^3$ ) 1 g of hydrochar with 4 g of  $\text{K}_2\text{CO}_3$  (Aldrich, 99 %) for SC800, or  $\text{KOH}$  (Panreac, 85 %) for SH800, for 2 h at room temperature, and then the samples were dried at  $100 \text{ }^\circ\text{C}$  in a ventilated oven. Activation occurred in a horizontal furnace (Thermolyne, model 21100) at  $800 \text{ }^\circ\text{C}$  for 1 h

under N<sub>2</sub> flow of 5 cm<sup>3</sup> s<sup>-1</sup> after a heating ramp of 10 °C min<sup>-1</sup>. Sample SC700P was prepared by physical impregnation of 1 g of hydrochar with 4 g of ground K<sub>2</sub>CO<sub>3</sub> and activated at 700 °C under the same experimental conditions as above. After cooling under N<sub>2</sub> flow, the samples were thoroughly washed with distilled water until pH 7, and finally dried overnight at 100 °C being cooled in a desiccator.

### Activated carbons characterization

Solids morphology characterization was made by scanning electron microscopy (SEM) images (JEOL, mod. 7001F) using an accelerating voltage of 25 kV.

The porous texture characterization of the carbon adsorbents was made by N<sub>2</sub> and CO<sub>2</sub> adsorption at -196 and 0 °C, respectively. The N<sub>2</sub> adsorption isotherms were obtained in an automatic apparatus Micromeritics ASAP 2010 while the CO<sub>2</sub> adsorption experiments were made in a conventional volumetric apparatus equipped with an MKS-Baratron (310BHS-1000) pressure transducer (0-133 kPa). In any case, before the isotherms measurement, the samples (~50 mg) were outgassed overnight at 120 °C under vacuum better than 10<sup>-2</sup> Pa (rotary/diffusion pump system). From N<sub>2</sub> adsorption data the apparent surface area ( $A_{\text{BET}}$ ) was determined through Brunauer-Emmett-Teller (BET) equation ( $0.05 < p/p^0 < 0.15$ )<sup>27</sup> and the total pore volume ( $V_{\text{total}}$ ) was assessed by the Gurvich rule,<sup>28</sup> corresponding to the volume of N<sub>2</sub> adsorbed at  $p/p^0 = 0.975$ . The microporosity was analysed applying the Dubinin–Radushkevich (DR) equation<sup>27</sup> to the N<sub>2</sub> and CO<sub>2</sub> adsorption data ( $W_{0 \text{ N}_2}$  and  $W_{0 \text{ CO}_2}$ , respectively). The  $\alpha_S$  method was also applied to the N<sub>2</sub> adsorption data, taking as reference the isotherm reported by Rodríguez-Reinoso et al.,<sup>29</sup> the volume of total micropores ( $V_{\alpha \text{ total}}$ ), ultramicropores ( $V_{\alpha \text{ ultra}}$ ) and supermicropores ( $V_{\alpha \text{ super}}$ ) were assessed according with the description presented in the ESI.† The mesoporous volume ( $V_{\text{meso}}$ ) corresponds to the difference between  $V_{\text{total}}$  and  $V_{\alpha \text{ total}}$ .

Densities of the activated carbons were determined by two distinct methodologies described in the literature.<sup>12, 15</sup> Tap density was measured by filling a graduated cylinder with the adsorbent and vibrating, while packing density was determined by pressing the adsorbent in a mould at a pressure of 550 kg cm<sup>-2</sup>. In all the cases, around 0.5 g were used to perform the assays. The measurements were repeated at least three times and the densities presented correspond to the mean value. The N<sub>2</sub> adsorption isotherms made with the samples obtained after packing revealed that apparent surface area decreases less than 10% after this procedure.

### **CH<sub>4</sub> and CO<sub>2</sub> adsorption measurements above atmospheric pressure**

The adsorption isotherms of CO<sub>2</sub> and CH<sub>4</sub> (Air Liquide, 99.995%), were determined in a laboratory made stainless steel volumetric apparatus, with a pressure transducer (Pfeiffer Vacuum, APR 266), equipped with a rotary/diffusion pump system which allowed a vacuum better than 10<sup>-2</sup> Pa. The apparatus and adsorption cell temperature was maintained with a water bath (Grant, GD 120) at 25.00 ± 0.05 °C. Before adsorption experiments, the samples were degassed as previously described for N<sub>2</sub> and CO<sub>2</sub> adsorption assays. The non-ideality of the gas phase was taken into account using the second and third Virial coefficients to calculate the adsorbed amounts. The selectivity and phase diagrams of binary CO<sub>2</sub> – CH<sub>4</sub> mixtures were estimated by a method based on the Ideal Adsorbed Solution Theory (IAST), which was detailed described in previous works<sup>9, 10</sup> and is summarized in the ESI.†

## **Results and discussion**

### **Activated carbons properties**

The activation of the sucrose-derived hydrochars with K<sub>2</sub>CO<sub>3</sub> and KOH at 800 °C originates adsorbents with well-developed porosity presenting type I isotherms



characteristic of microporous solids (Figure 1(a)). The sample physically impregnated with  $K_2CO_3$  and activated at 700 °C (SC700P) is, as expected, the carbon with the less developed microporous structure, while KOH activation led to the material with the most developed micropore network. Activation with KOH produces a material with the highest specific surface area and pore volumes (Table 1). However, when compared with the  $K_2CO_3$ -activated carbons, SH800 sample presents the lowest preparation yield (13% *versus* 45-51 %) and is the only that did not maintain the spherical shape of the hydrochar (Figure 2).

According to the literature, KOH activation mechanism involves a series of reactions that start at temperatures relatively low ( $\sim 400$  °C) leading to the formation of  $H_2O$ ,  $CO_2$ ,  $CO$  and  $H_2$ .<sup>30-32</sup> Some of these compounds are commonly used as physical activating agents and so the consumption of the carbon matrix starts at  $\sim 400$  °C. Another reaction product of KOH activation is  $K_2CO_3$  that will decompose only at temperatures between 700 and 800 °C, resulting in the formation of metallic K, which remains intercalated in the carbon structure. The activation occurs due to redox reactions where C from the carbon matrix is oxidized and the activating agent is reduced (from  $K^+$  to metallic K). The removal of metallic K during the washing step unblock the micropore network.

When  $K_2CO_3$  is used as activating agent the reaction starts only at around 800 °C<sup>30</sup> and the reactions at lower temperatures observed in the case of KOH are absent. The use of carbonate will then allow a less extensive consumption of the carbon matrix resulting in a lower porosity development, but gathering the conditions to maximize the material density. Thus, the higher activation yield, less extensive development of the microporous network (Table 1) and the preservation of hydrochar spherical morphology (Figure 2) observed for the  $K_2CO_3$ -activated carbons (SC800 and SC700P) are in line

with differences between the activation mechanism of  $K_2CO_3$  and KOH and reveal the advantages of  $K_2CO_3$  activation of spherical hydrochars.

Regarding the microporous structure, the  $\alpha_s$  method results (Table 1) show that while the sample activated with KOH (SH800) has exclusively larger micropores (supermicropores – widths between 0.7 and 2 nm), the  $K_2CO_3$ -activated carbons present both narrow and wider micropores, with higher percentage of narrow micropores (ultramicropores – widths < 0.7 nm). These results are expected according to the distinct activation mechanisms.

The volumes of micropores assessed applying the DR equation to the  $N_2$  and  $CO_2$  data are also in line with the previous analysis: sample SH800 has  $W_{0\ N_2} > W_{0\ CO_2}$ , which is indicative of high activation degrees and the presence of wider micropores, while samples activated with  $K_2CO_3$  (SC800 and SC700P) have  $W_{0\ N_2} < W_{0\ CO_2}$ , which is indicative of the presence of narrower micropores.<sup>33</sup> Further characterization of the activated carbons by micropore size distributions (Figure 1(b)), assessed by fitting  $CO_2$  adsorption data at 0 °C to the method described by Pinto et al.,<sup>34</sup> corroborate the assumptions made above. Carbon SH800 has a bimodal micropore size distribution with pores mainly in the supermicropore region, whereas samples SC800 and SC700P present monomodal distributions centered at ~ 0.7 and ~ 0.5 nm, respectively. It is noteworthy that carbon SC800 has a broad distribution of pores around 0.8 nm that are considered to maximize methane uptake and its delivery at ambient pressure.<sup>12</sup> Although presenting the less developed porous network, sample SC700P has a very narrow micropore size distribution which, as it will be discussed later on, plays a very important role in the separation of  $CO_2/CH_4$  mixture.

Envisaging the use of these samples for carbon storage, it is also essential to evaluate their density, because the materials used for gas storage must also have high storage capacity on a volumetric basis. Both tap and packing density values are presented in Table 2, and reveal that  $K_2CO_3$ -activated carbons have much higher densities. In the case of packing densities, the values determined for the  $K_2CO_3$ -activated samples are two to three times higher than that obtained for the sample activated with KOH.

Summarizing, although presenting lower micropore volumes than sample activated with KOH, the carbons prepared by  $K_2CO_3$  activation of the hydrochar have preparation yields about four times higher and very high packing densities, most certainly related with the preservation of the spherical morphology after the activation, allied to monomodal micropore size distributions centered below 0.8 nm; being all these features fundamental requisites for materials to be used in gas storage.

### **Methane and carbon dioxide adsorption**

The adsorption isotherm profiles of  $CH_4$  and  $CO_2$ , up to 1000 kPa (Figure 3), show that sample SC700P seems to be reaching a plateau at high pressures, indicating a saturation of the porosity, for the adsorption of both gases. For the other two samples, especially in the case of SH800, the materials are not saturated at the highest pressures attained. This indicates that the highest pressure used was sufficient to saturate the material with the narrower pores (SC700P), but not the other two materials which have wider pores (SH800 and SC800).

The highest uptake for  $CO_2$  was attained by sample SH800, which is in line with the significantly higher apparent surface area and pore volume of this sample comparing to the others (Table 1). For the  $K_2CO_3$ -activated carbons the maximum adsorbed amounts also follow the surface area and pore volume trend. On the contrary, in the low pressure

region carbon SH800 presents lower CO<sub>2</sub> uptakes (~25%) than the K<sub>2</sub>CO<sub>3</sub>-activated carbons (Figure S2). This behaviour is probably a consequence of the wider micropores of this sample (Figure 1 and Table 1), which are not so effectively interacting with the CO<sub>2</sub> molecules in the low pressure region. This issue is further discussed below.

The results of CH<sub>4</sub> adsorption present a different trend from those of CO<sub>2</sub>, in the studied pressure range. Carbon SC800 adsorbed higher amounts than the other samples, although it seems likely from the isotherms configuration that the isotherm of SH800 will cross the isotherm of SC800 at higher pressures than those tested. This crossing is observed for CO<sub>2</sub> adsorption, at pressures around 300 kPa.

The lines on Figure 3 represent the fitting of the Virial equation (equation 1 in ESI†). The Henry's constant ( $K$ ) quantifies the initial slope of the isotherms and is directly connected with the affinity of the surface for the gas molecules. Thus, the results for  $K$  presented on Table 3 quantify the affinity of the materials for CH<sub>4</sub> and CO<sub>2</sub>, which were already commented above. In the CH<sub>4</sub> case, the values follow the order SC800>SC700P>SH800 and for CO<sub>2</sub>, the order is SC700P>SC800>SH800, with K<sub>2</sub>CO<sub>3</sub>-activated carbons always showing higher affinity for both gases than KOH-activated carbon. The  $K$  values obtained for CH<sub>4</sub> (Table 3) are above the average value reported by Matranga et al.<sup>35</sup> for a large set of experimental data ( $1.2 \times 10^{-2}$  mol kg<sup>-1</sup> kPa) and above that from simulation data ( $0.7 \times 10^{-2}$  mol kg<sup>-1</sup> kPa), indicating that all obtained samples have a considerable number of active adsorption sites that favor CH<sub>4</sub> adsorption.

Considering the pore network characteristics (Figure 1 and Table 1), it seems that the sample with the narrower pores (SC700P) is more effective for high CO<sub>2</sub> adsorption at low pressures (highest  $K$  value for CO<sub>2</sub>, Table 3), while the sample with intermediate micropores (SC800) is more effective for CH<sub>4</sub> adsorption at low pressures (highest  $K$

value for CH<sub>4</sub>, Table 3). In fact, the much high value of  $K$  found for the adsorption of CO<sub>2</sub> on SC700P indicates that materials with narrow distributions around 0.5 nm are important for the initial high uptake of this gas. The SC800 case, with the highest value of  $K$  for CH<sub>4</sub> adsorption, indicates that materials with pores distributions round 0.6-0.9 nm are more suitable for adsorption of CH<sub>4</sub>. Considering the critical molecular size of CO<sub>2</sub> and CH<sub>4</sub>, 0.34 nm and 0.38 nm, respectively, one can speculate that in this type of carbon materials CO<sub>2</sub> is more prone to adsorb in the pores in a single layer fashion, while CH<sub>4</sub> is more prone to adsorb in a double layer fashion.

It has been shown that pores below about 0.7 nm are the ones involved in CH<sub>4</sub> adsorption in activated carbons.<sup>11</sup> However, simulation of CH<sub>4</sub> adsorption on an ideal porous graphite revealed that a pore size of around 0.8 nm is more effective to achieve the highest density of CH<sub>4</sub> adsorbed,<sup>35</sup> giving a theoretical adsorbed amount around 7 mmol g<sup>-1</sup> at 1000 kPa. Our best result at 1000 kPa (5.5 mmol g<sup>-1</sup>) is lower than this maximum theoretical value at this pressure and also lower than the value reported for anthracite derived activated carbons optimized for CH<sub>4</sub> storage (7 mmol g<sup>-1</sup>),<sup>12</sup> although it is significantly higher than previous reported values for several types of activated carbons (2.5 – 4.5 mmol g<sup>-1</sup>).<sup>35</sup> Nevertheless, when a carbon density similar to that found on activated carbons (lower than graphite) is used in the simulation of CH<sub>4</sub> adsorption, the values obtained for adsorbed amounts are about 12% lower<sup>36</sup> and closer to that measured in our best result for sample SC800.

It should be noted that the agreement between the best theoretical pore size (0.8 nm) and the experimental results shown here for CH<sub>4</sub> adsorption also indicates that the method chosen<sup>34</sup> to obtain the micropore size distributions is giving meaningful data. Previous attempts using the Dubinin–Stoeckli method to calculate micropore size distributions did not give this agreement,<sup>12</sup> probably due to the predefined Gaussian distribution

underlying the Dubinin–Stoeckli method that is not assumed in the method followed in this work.<sup>34</sup>

### Selectivity for CO<sub>2</sub>/CH<sub>4</sub> mixtures and CH<sub>4</sub> storage

Selectivity and phase diagrams of the separation of CO<sub>2</sub>/CH<sub>4</sub> mixtures were estimated from the Virial equations, using a method based on Ideal Adsorbed Solution Theory (IAST) detailed elsewhere<sup>9, 10</sup> and briefly summarized in the ESI.† For the SC800 and SH800 samples, the selectivity of the separation is similar in all pressure range (Figure 4). The carbon SC700P presents an initial selectivity close to 7 and then decreases to 4, increasing again with rising pressure to about 6, at 1000 kPa. It is important to emphasize that, although SC700P presents modest adsorbed amounts compared to the other samples (Figure 3), the selectivity of the separation on this sample is significantly better. In fact, this carbon presents a selectivity that is above the value of 3 that is considered as reference for industrial feasibility,<sup>37</sup> while the other samples only reach close to this value at the highest pressure tested. The difference among samples is further illustrated in Figure 5 where it can be seen that the SC700P presents an improved performance over the other samples. For example, considering the separation of a gas mixture with 0.5 molar composition ( $y_{\text{CH}_4}$ ), typical of bio and landfill gases, the composition in adsorbed phase ( $x_{\text{CH}_4}$ ) is 0.15 on SC700P and about 0.25 on SH800 and SC800, at 500 kPa and 25°C. This means that the adsorbed phase on SC700P is richer in CO<sub>2</sub> (0.85) than that on SH800 and SC800 (0.75). Clearly, the narrow pores size distribution of SC700P sample is responsible for the interesting selectivity for the mixture separation.

For applications, it is often useful to compare the adsorbents regarding their gas storage capacity as the volume of gas retained in the material per volume of storage vessel or separation column. The importance of the density on the evaluation of the volumetric storage capacity of a given material was recently highlighted in a work of Kunowsky et

al.<sup>38</sup> For this kind of comparison, in our work the packing density has been taken into account to express the adsorbed amounts per volume of adsorbent material. When the adsorbed amounts are converted to gas volume (Standard Temperature and Pressure - STP), the volume of gas retained in a given adsorbent volume can be calculated in a V/V basis. These results show a very different trend of the isotherms (Figure 6). Comparing with previously presented isotherms with adsorbed amount expressed per gram of material (Figure 3), it can be seen that the KOH-activated sample (SH800) presents a significant decrease in the in the volume adsorbed (Figure 6) for both gases, in relation to the K<sub>2</sub>CO<sub>3</sub>-activated carbons, due to its much lower packing density among the materials (Table 2). So, although presenting the highest adsorbed amounts per gram of samples (Figure 3), the low packing density of carbon SH800 makes it unsuitable for some applications, where the volume of the adsorbent material is a limiting factor, as is the case of gas storage.

The curves in V/V (Figure 6) highlight the potentialities of the K<sub>2</sub>CO<sub>3</sub>-activated samples, as they present significantly higher volumes adsorbed per volume of material than the sample activated with KOH. It is well known that KOH activation tends to give activated carbons with high surface areas and essentially microporous. However, in the particular case of sucrose-derived hydrochars, the KOH destroys the spherical structure of the hydrochar (Figure 2) hindering an efficient packing of the particles, thus giving low packing densities. K<sub>2</sub>CO<sub>3</sub> appears to be a better activating agent because the spherical structure is maintained and still gives high surface areas (Table 1). The combination of these two features gives K<sub>2</sub>CO<sub>3</sub> activated hydrochars an enhanced storage capacity (V/V) when compared to KOH activation reported in this work and in a previously published study.<sup>13</sup> In fact, the best CH<sub>4</sub> storage value obtained in the present work for SC800 sample (90 (V/V), Table 2) at 1000 kPa is higher than those reported by Falco et al.<sup>13</sup> (between

43 and 53 (V/V), both values calculated from reported adsorbed amounts 1000 kPa and the packing densities) and interestingly similar to those observed on anthracite derived carbons activated with KOH (82 (V/V))<sup>12</sup>, at the same pressure. Comparing the storage capacity (Table 2) and the surface area (Table 1) of the materials, it is evident that surface area is not the only parameter ruling the CH<sub>4</sub> storage capacity. This is due to the influence of the packing density, already discussed, and also to the lower density of CH<sub>4</sub> in supermicropores<sup>11</sup> present in the material with the highest surface area (SH800).

Considering the upgrade of natural, landfill or biogas, the activated carbons can be evaluated regarding the composition of the adsorbed phase. For this, the volume of each gas adsorbed (V/V) was estimated as function of the composition of the gas phase (Figure 7). Once again, the KOH-activated carbon (SH800) presents lower adsorbed volumes than the K<sub>2</sub>CO<sub>3</sub>-activated carbons (SC800 and SC700P). More interesting is the performance of the SC700P sample that presents a combination of high CO<sub>2</sub> adsorbed volumes and an adsorbed phase richer in CO<sub>2</sub> in a wide range of gas composition. A detailed comparison of the plots in Figure 7 shows that the crossing point at which the concentration of CO<sub>2</sub> in the adsorbed phase becomes lower than that of CH<sub>4</sub>, is obtained at higher molar fraction of CH<sub>4</sub> in the gas phase (0.85) for the SC700P sample. This means that, during CO<sub>2</sub>/CH<sub>4</sub> separation, this sample will retain more CO<sub>2</sub> than CH<sub>4</sub> in a wider range of feed compositions than the other tested samples. For practical applications, although K<sub>2</sub>CO<sub>3</sub>-activated carbon SC700P presents lower adsorbed amounts per grams and lower surface area and pores volumes, due to its high density and selectivity it appears as the most promising material for CO<sub>2</sub>/CH<sub>4</sub> separation.



## Conclusions

$K_2CO_3$  activation of sucrose-derived hydrochars allows the preparation of materials preserving the microspherical morphology, along with high porosity development and specific properties suitable to be used in  $CO_2/CH_4$  separation. Moreover, the spherical morphology leads to high packing densities, a crucial parameter for high gas storage volume (V/V); being particularly important for  $CH_4$  storage. Conversely, KOH activated sample (SH800) has lower preparation yield and density that leads to lower storage volumes (V/V) and wider micropores less favourable for  $CO_2/CH_4$  separation.

Furthermore, the micropore size distributions assessed from  $CO_2$  adsorption data without imposing a Gaussian distribution, reveal that the sample presenting the best  $CH_4$  adsorption capacity (SC800) is also the one for which the maximum is centered in the predicted pore width for enhance  $CH_4$  storage (0.8 nm). Considering the micropore size distribution, it seems that the microspherical activated carbon (SC700P) with narrow pore distribution centered at 0.5 – 0.6 nm is more suitable for application in the  $CO_2/CH_4$  separation.

Besides the applications herein described, the properties of  $K_2CO_3$ -activated hydrochar samples allow to envisage their use in other processes. These carbons combine the spherical morphology with very narrow micropore size distributions, so they can present molecular sieves properties. On the other hand, their acidic surface chemistry opens new possibilities to their use in other adsorption processes or for the synthesis of functional carbon-based materials.

## Acknowledgments

The authors thank Fundação para a Ciência e Tecnologia, Portugal, for financial support through projects PEst-OE/QUI/UI0100/2013 (CQB) and Pest-

C/EQB/LA0006/2011(REQUIMTE) and Operation NORTE-07-0124-FEDER-000067 – NANO CHEMISTRY. ASM thanks FCT for the Post-doc grant SFRH/BPD/86693/2012. MLP thanks FEDER, QREN, COMPETE, and FCT for financial support to CICECO project FCOMP-01-0124-FEDER-037271 (PEst-C/CTM/LA0011/2013) and Investigador FCT contract IF/00993/2012/CP0172/CT0013.

## References

1. J. Bekkering, A. A. Broekhuis and W. J. T. van Gernert, *Bioresource Technol.*, 2010, **101**, 450-456.
2. K. S. Knaebel and H. E. Reinhold, *Adsorption*, 2003, **9**, 87-94.
3. S. Matar and L. F. Hatch, *Chemistry of Petrochemical Processes*, Gulf Publishing Company, Houston, 2000.
4. P. Weiland, *Appl. Microbiol. Biot.*, 2010, **85**, 849-860.
5. *Commission Directive 2001/27/EC of 10 April 2001*.
6. W. T. Tsai, *Renew. Sust. Energ. Rev.*, 2007, **11**, 331-344.
7. W. Qin, F. N. Egolfopoulos and T. T. Tsotsis, *Chem. Eng. J.*, 2001, **82**, 157-172.
8. V. K. Saini, M. Pinto and J. Pires, *Green Chem.*, 2011, **13**, 1251-1259.
9. J. Pires, V. K. Saini and M. L. Pinto, *Environ. Sci. Technol.*, 2008, **42**, 8727-8732.
10. M. L. Pinto, J. Pires and J. Rocha, *J. Phys. Chem. C*, 2008, **112**, 14394-14402.
11. J. Alcañiz-Monge, D. Lozano-Castelló, D. Cazorla-Amorós and A. Linares-Solano, *Micropor. Mesopor. Mat.*, 2009, **124**, 110-116.
12. D. Lozano-Castelló, D. Cazorla-Amorós, A. Linares-Solano and D. F. Quinn, *Carbon*, 2002, **40**, 989-1002.

13. C. Falco, J. P. Marco-Lozar, D. Salinas-Torres, E. Morallón, D. Cazorla-Amorós, M. M. Titirici and D. Lozano-Castelló, *Carbon*, 2013, **62**, 346-355.
14. M. Sevilla and A. B. Fuertes, *Energ. Environ. Sci.*, 2011, **4**, 1765-1771.
15. M. Jorda-Beneyto, D. Lozano-Castello, F. Suarez-Garcia, D. Cazorla-Amoros and A. Linares-Solano, *Micropor. Mesopor. Mat.*, 2008, **112**, 235-242.
16. M. Galhetas, A. S. Mestre, M. L. Pinto, I. Gulyurtlu, H. Lopes and A. P. Carvalho, *Chem. Eng. J.*, 2014, **240**, 344-351.
17. A. S. Mestre, A. S. Bexiga, M. Proença, M. Andrade, M. L. Pinto, I. Matos, I. M. Fonseca and A. P. Carvalho, *Bioresource Technol.*, 2011, **102**, 8253-8260.
18. I. Cabrita, B. Ruiz, A. S. Mestre, I. M. Fonseca, A. P. Carvalho and C. O. Ania, *Chem. Eng. J.*, 2010, **163**, 249-255.
19. A. S. Mestre, J. Pires, J. M. F. Nogueira and A. P. Carvalho, *Carbon*, 2007, **45**, 1979-1988.
20. A. P. Carvalho, M. Gomes, A. S. Mestre, J. Pires and M. Brotas de Carvalho, *Carbon*, 2004, **42**, 672-674.
21. A. S. Mestre, R. A. Pires, I. Aroso, E. M. Fernandes, M. L. Pinto, R. L. Reis, M. A. Andrade, J. Pires, S. P. Silva and A. P. Carvalho, *Chem. Eng. J.l*, 2014, **253**, 408-417.
22. M. A. Andrade, R. J. Carmona, A. S. Mestre, J. Matos, A. P. Carvalho and C. O. Ania, *Carbon*, 2014, **76**, 183-192.
23. M. Galhetas, A. S. Mestre, M. L. Pinto, I. Gulyurtlu, H. Lopes and A. P. Carvalho, *J. Colloid Interf. Sci.*, 2014, Doi: <http://dx.doi.org/10.1016/j.jcis.2014.06.043>
24. A. S. Mestre, C. Freire and A. P. Carvalho, *EcoCarbons: Hydrothermal carbonization of carbohydrates*, Abstracts of the XXXIV Reunión Bienal Real Sociedad Española de Química (Oral presentation), Santander (Spain), 2013.
25. D. Adinata, W. M. A. W. Daud and M. K. Aroua, *Bioresource Technology*, 2007, **98**, 145-149.

26. H. Marsh and F. Rodríguez-Reinoso, *Activated Carbon*, Elsevier, Oxford, 2006.
27. S. J. Gregg and K. S. W. Sing, *Adsorption, Surface Area and Porosity*, Academic Press Inc., London, 1982.
28. L. Gurvich, *J. Phys. Chem. Soc. Russ.*, 1915, **47**, 805-827.
29. F. Rodriguez-Reinoso, J. M. Martin-Martinez, C. Prado-Burguete and B. McEnaney, *J. Phys. Chem.*, 1987, **91**, 515-516.
30. J. Wang and S. Kaskel, *J. Mater. Chem.*, 2012, **22**, 23710-23725.
31. D. Lozano-Castello, J. M. Calo, D. Cazorla-Amoros and A. Linares-Solano, *Carbon*, 2007, **45**, 2529-2536.
32. E. Raymundo-Pinero, P. Azais, T. Cacciaguerra, D. Cazorla-Amoros, A. Linares-Solano and F. Beguin, *Carbon*, 2005, **43**, 786-795.
33. F. Rodríguez-Reinoso, in *Carbon and Coal Gasification: Science and Technology*, eds. J. L. Figueiredo and J. A. Moulijn, Martinus Nijhoff, Dordrecht, 1986.
34. M. L. Pinto, A. S. Mestre, A. P. Carvalho and J. Pires, *Ind. Eng. Chem. Res.*, 2010, **49**, 4726-4730.
35. K. R. Matranga, A. L. Myers and E. D. Glandt, *Chem. Eng. Sci.*, 1992, **47**, 1569-1579.
36. X. S. Chen, B. McEnaney, T. J. Mays, J. Alcaniz-Monge, D. Cazorla-Amoros and A. Linares-Solano, *Carbon*, 1997, **35**, 1251-1258.
37. R. T. Yang, *Gas Separation by Adsorption Processes*, Butterworths Publishers, Boston, 1987.
38. M. Kunowsky, F. Suarez-Garcia and A. Linares-Solano, *Micropor. Mesopor. Mater.*, 2013, **173**, 47-52.

**Table 1.** Nanotextural properties of the activated carbons and preparation yield ( $\eta$ ).

Sample	$A_{\text{BET}}$ ( $\text{m}^2 \text{g}^{-1}$ )	$V_{\text{total}}^{\text{a}}$ ( $\text{cm}^3 \text{g}^{-1}$ )	$V_{\text{meso}}^{\text{b}}$ ( $\text{cm}^3 \text{g}^{-1}$ )	$\alpha_s$ Method			DR Equation		$\eta^{\text{c}}$ (%)
				$V_{\alpha \text{ total}}$ ( $\text{cm}^3 \text{g}^{-1}$ )	$V_{\alpha \text{ ultra}}$ ( $\text{cm}^3 \text{g}^{-1}$ )	$V_{\alpha \text{ super}}$ ( $\text{cm}^3 \text{g}^{-1}$ )	$W_{\text{DR N}_2}$ ( $\text{cm}^3 \text{g}^{-1}$ )	$W_{\text{DR CO}_2}$ ( $\text{cm}^3 \text{g}^{-1}$ )	
SH800	2431	1.14	0.06	1.08	0.00	1.08	0.90	0.71	13
SC800	1375	0.63	0.01	0.62	0.35	0.27	0.58	0.65	45
SC700P	694	0.31	0.00	0.31	0.23	0.08	0.31	0.41	51

<sup>a</sup> evaluated at  $p/p^0 = 0.975$  in the  $\text{N}_2$  adsorption isotherms at  $-196$  °C.

<sup>b</sup> difference between  $V_{\text{total}}$  and  $V_{\alpha \text{ total}}$ .

<sup>c</sup> yield is defined as: g of activated carbon per 100 g of hydrochar.

**Table 2.** Tap and packing densities of the activated carbons. Calculated methane and carbon dioxide uptake at 1000 kPa and 25 °C (volume of methane or carbon dioxide adsorbed per volume of sample considering the packing density: V/V).

<b>Sample</b>	<b><i>Tap</i> density (g cm<sup>-3</sup>)</b>	<b><i>Packing</i> density (g cm<sup>-3</sup>)</b>	<b>CH<sub>4</sub> uptake (V/V)</b>	<b>CO<sub>2</sub> uptake (V/V)</b>
SH800	0.07	0.36	40	99
SC800	0.34	0.79	90	164
SC700P	0.42	0.92	65	108

**Table 3.** Virial coefficients and Henry constants for the adsorption of methane and carbon dioxide on the activated carbons.<sup>a</sup>

Gas	Sample	$K$ (mol kg <sup>-1</sup> kPa <sup>-1</sup> )	$C_1$ (kg mol <sup>-1</sup> )	$C_2$ (kg mol <sup>-1</sup> ) <sup>2</sup>	$C_3$ (kg mol <sup>-1</sup> ) <sup>3</sup>
CH <sub>4</sub>	SH800	$1.67 \times 10^{-2}$	0.272	-0.014	-
	SC800	$3.13 \times 10^{-2}$	0.313	-	-
	SC700P	$2.61 \times 10^{-2}$	0.315	0.090	-
CO <sub>2</sub>	SH800	$3.98 \times 10^{-2}$	0.117	-0.002	-
	SC800	$7.85 \times 10^{-2}$	0.380	-0.050	0.004
	SC700P	$28.3 \times 10^{-2}$	1.961	-0.637	0.078

<sup>a</sup> Obtained by the nonlinear least-squares fit of equation 1 of ESI† to the adsorption data.

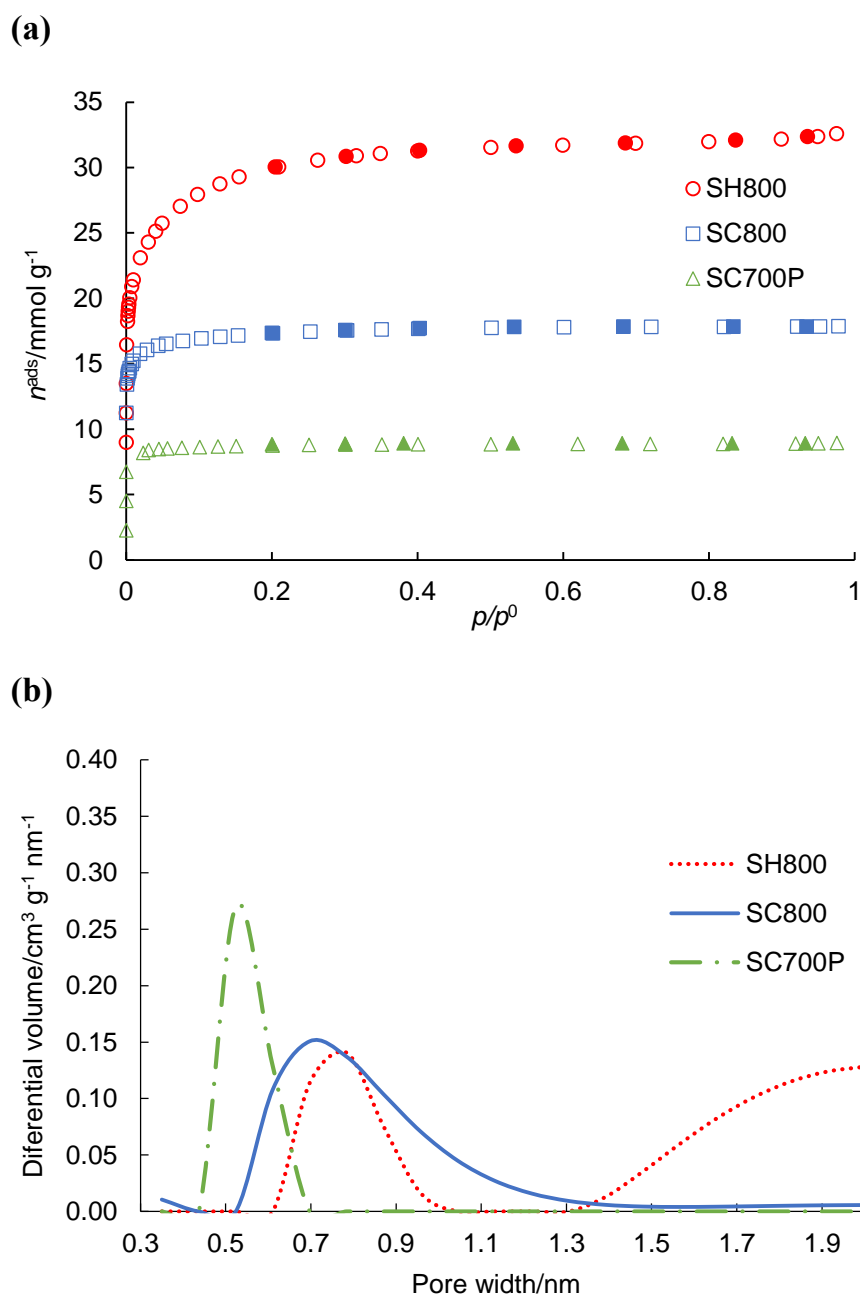


**Figure 1.** (a) N<sub>2</sub> adsorption-desorption isotherms at -196 °C, closed symbols are the desorption points; (b) Micropore size distributions of the activated carbon, obtained by fitting CO<sub>2</sub> adsorption data at 0 °C to the method described by Pinto et al..<sup>34</sup>



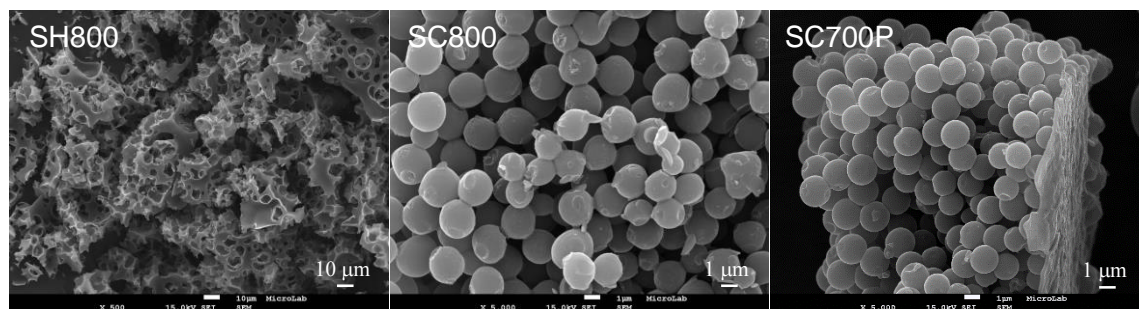


**Figure 2.** SEM images of the activated carbon samples.

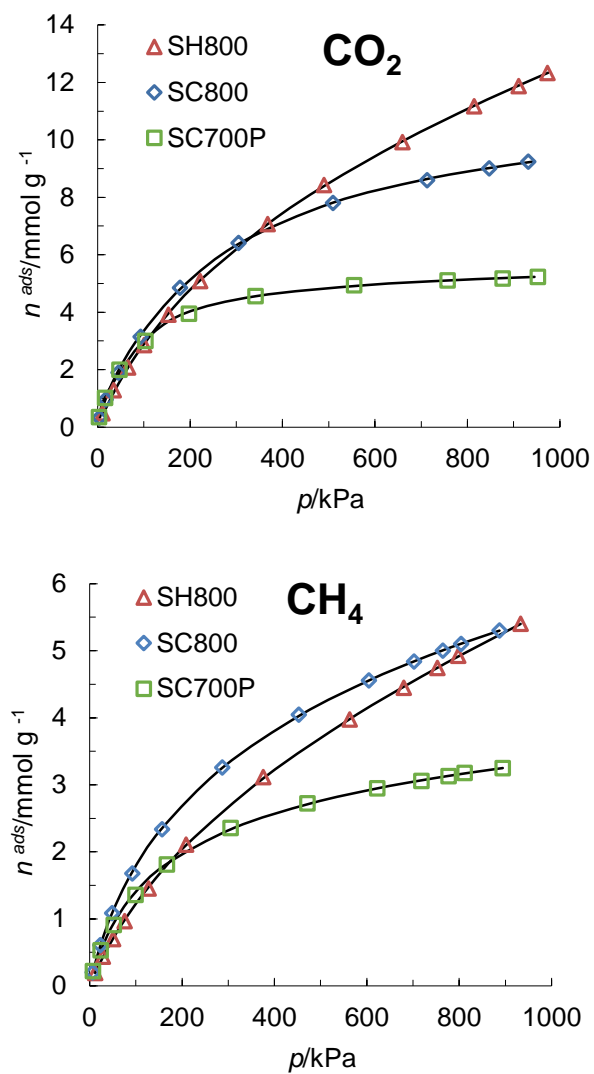


**Figure 3.** Carbon dioxide and methane and adsorption isotherms at 25 °C on the activated carbons. The lines represent the fitting of the Virial equation.

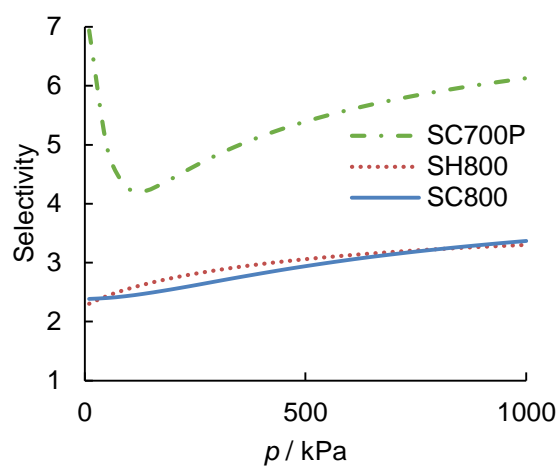


**Figure 4.** Average selectivity for the  $\text{CO}_2/\text{CH}_4$  separation on the activated carbons.

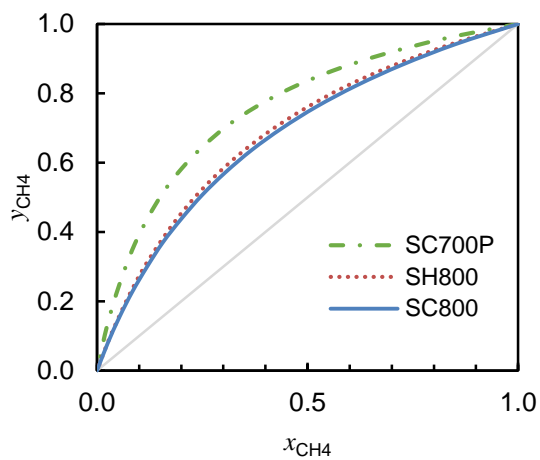


**Figure 5.** Isothermal (25 °C), isobaric (500 kPa)  $xy$  phase diagrams of the  $\text{CO}_2/\text{CH}_4$  mixtures on the activated carbons.  $y_{\text{CH}_4}$  is the molar fraction of methane in the gas phase;  $x_{\text{CH}_4}$  is the molar fraction of methane in the adsorbed phase.

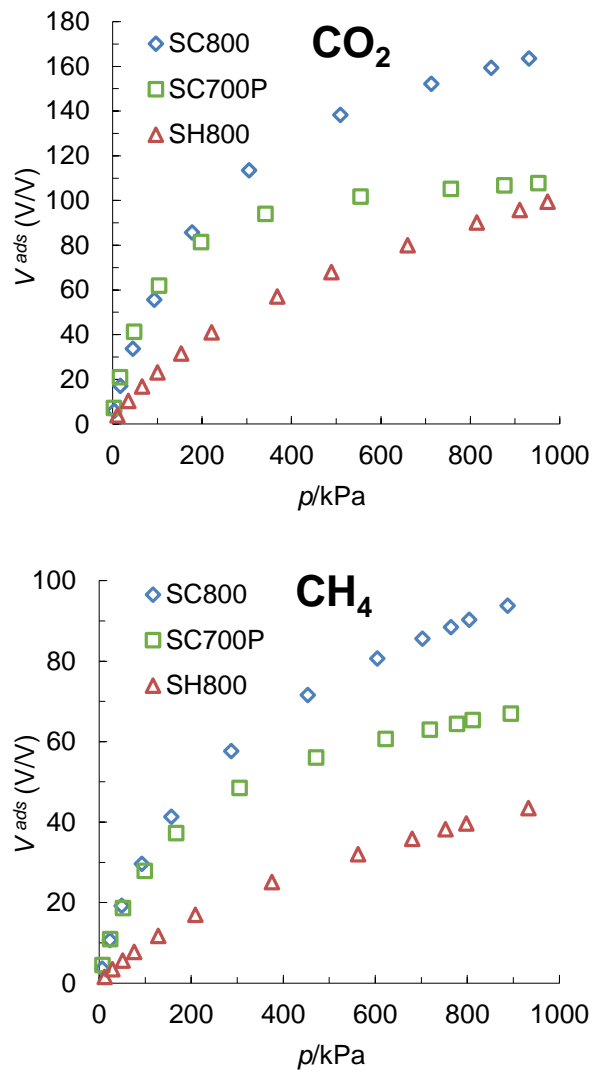


**Figure 6.** Carbon dioxide and methane adsorption isotherms at 25 °C on the activated carbons, taking in to the account the density of the materials and expressing the amounts adsorbed per unit volume of material.

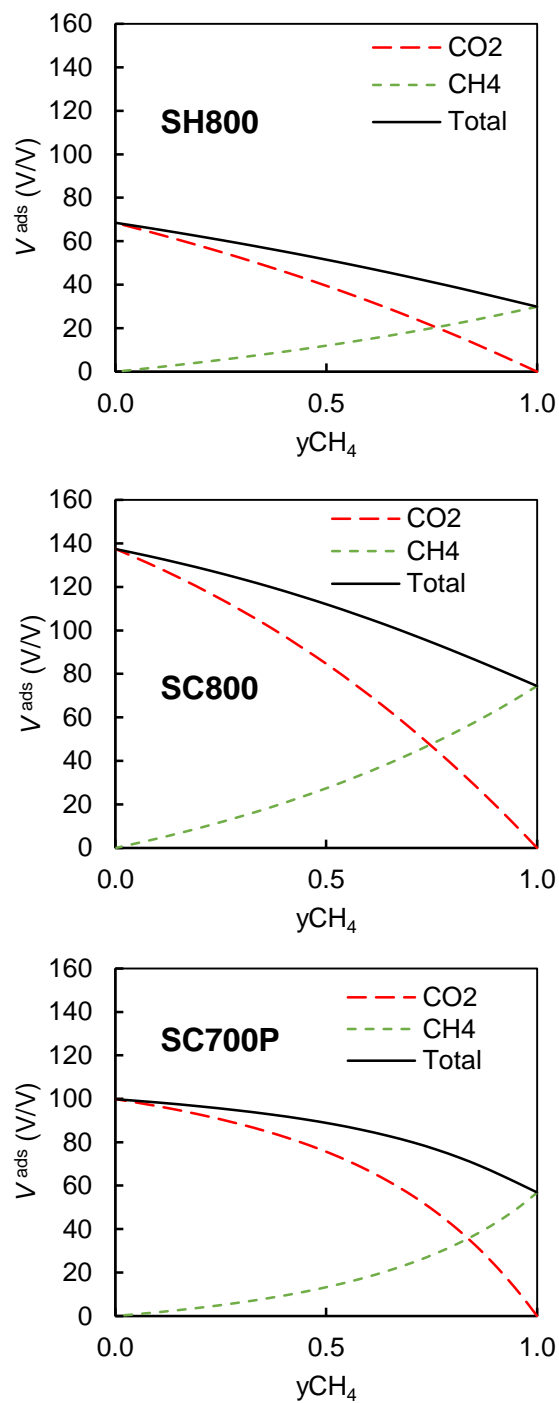


**Figure 7.** Adsorbed amounts of the CO<sub>2</sub>/CH<sub>4</sub> mixture as a function of the CH<sub>4</sub> molar fraction in the gas phase, at 500 kPa and 25 °C, for the activated carbons.

**TABLE OF CONTENTS**

Microspherical  $\text{K}_2\text{CO}_3$ -activated carbons for methane storage or biogas upgrade: high surface areas and packing density, tuneable microporosity, and  $\text{CO}_2/\text{CH}_4$  selectivity.

